Measuring the volumes and thickness of hippocampal subfields in vivo using automatic segmentation of T2-weighted MRI: A pilot evaluation study

P. A. Yushkevich[1], H. Wang[1], J. Pluta[1], S. R. Das[1], B. Avants[1], M. Weiner[2], S. Mueller[2], and D. Wolk[3]

[1]PICSL, Department of Radiology, University of Pennsylvania, Philadelphia, PA, United States, [2]Department of Radiology, University of California, San Francisco, San Francisco, CA, United States, [3]Department of Neurology, University of Pennsylvania, Philadelphia, PA, United States

Purpose: *We demonstrate that meaningful cross-sectional differences in the subfields of the hippocampal formation (HF) can be detected in patients with mild cognitive impairment (MCI) using automatic segmentation of focal T2-weighted MRI.* Boundaries between the layers and subfields of the HF are virtually indistinguishable in routine 1 mm^3 T1-weighted MRI at 1.5 and 3 Tesla. However, mounting evidence suggests that focal fast spin echo MRI tailored for HF imaging (HF-MRI for short) provides sufficient contrast between the HF layers to allow reliable measurement of change in HF subfields. Cross-sectional differences in HF subfield volumes measured in HF-MRI have recently been shown to be consistent with the topography of neuropathology in several brain disorders, including AD and MCI [1,2,3]. However, until now, analysis of HF subfields in HF-MRI required prohibitively expensive manual segmentation (3-4 hours per image). Our group developed an automatic method for subfield segmentation in HF-MRI. Its accuracy for the larger subfields (CA1, dentate gyrus) is comparable to the best results reported for whole HF segmentation. In the present work, we evaluate the ability of this method to detect subfield-specific differences between MCI patients and matched healthy controls. *To our knowledge, these are the first reported results of subfield-specific HF morphometry using automatic analysis of HF-MRI, a modality recognized as superior for HF imaging.*

Methods: Subjects and Imaging. HF-MRI was obtained in a cohort of amnestic MCI patients (n=9; mean age: 66.7; mean MMSE: 27.6) and healthy controls (n=17; mean age: 70.4; mean MMSE: 29.4) taking part in an ongoing study at Penn. Scans were performed on a 3 Tesla Siemens Trio using an 8-channel head coil and a body coil transmitter. HF-MRI were acquired with the fast spin echo sequence (TR/TE=5310/73 ms; 30 oblique slices orthogonal to the main axis of the HF; FOV=220 mm x 220 mm; 2 mm thickness; 0.6 mm gap; 448 x 358 matrix; 2 averages), yielding focal images with 0.5 x 0.6 x 2.6 mm^3 resolution. Automatic Segmentation. Segmentation uses the multi-atlas label fusion approach in [4], which relies on several free image analysis tools and is itself freely available (www.nitrc.org/projects/ashs). A set of HF-MRI acquired at 4 Tesla at the San Francisco VA Medical Center were segmented manually and used as atlases. The manual segmentation includes subfields CA1, CA2, CA3, dentate gyrus (DG), subiculum (SUB), entorhinal cortex (ERC), which are labeled in 4-6 HF-MRI slices that span the body of the HF. Additional labels HEAD, TAIL, parahippocampal gyrus (PHG) are assigned to voxels in and near the HF outside of these 4-6 slices, where subfield differentiation is unreliable due to complex anatomy and bending of the HF out of the slice plane. Each atlas was co-registered to each target HF-MRI using linear global registration (FLIRT tool in FSL library [5]) and non-linear deformable registration (SyN tool in ANTS library [6]). A local similarity-weighted voting strategy was used to compute a consensus segmentation of the target image. Consensus segmentations were further postprocessed using a machine learning algorithm [4], which uses training data to learn the local intensity patterns associated with the voxels where the consensus segmentation disagrees with the manual segmentation, and then finds and relabels such voxels in the target image. The segmentation algorithm requires minimal manual input in the form of identifying the 4-6 slices that span the body of each HF in the target image. Morphometry. Normalized subfield volumes and thickness are compared across groups. The volume of each subfield is divided by the number of slices spanned by the HF body to account for variability in the latter, then normalized by the intracranial volume. Thickness is computed at each point of each subfield using a "fuzzy" 3D distance transform algorithm. Thickness maps are spatially normalized to allow pointwise comparison between groups.

Results: Segmentation Accuracy. Examples of automatic segmentation results are shown in Figure 2. The accuracy of the automatic algorithm was previously evaluated in a leave-N-out experiment conducted on the HF-MRI images used as atlases. Dice overlap between manual and automatic segmentations exceeded 0.87 for CA1, DG and HEAD; and was above 0.75 for SUB, ERC and TAIL. Similar evaluation on HF-MRI Penn data has not yet been done, and accuracy may be lower due to scanner/protocol differences between the atlases and target images. Group Differences. Average subfield thickness maps for the MCI and control cohorts are plotted in Figure 3 (the DG is excluded from the plot for better visualization). CA1 is thicker in controls than in MCI patients. Statistical comparison of subfield volumes reveals most significant differences in the left CA1 subfield, followed by the left DG (Figure 3). By contrast, whole HF volume differences did not reach significance.

Discussion: The main finding, i.e., highly significant difference in the CA1 subfield, is consistent with the known topography of AD neurodegeneration. The fact that changes in CA1 were more significant than whole HF volume point to the potential improved sensitivity of subfield-specific measures derived from HF-MRI. The ability to detect significant effects of MCI on a very small dataset points to the efficacy of automatic HF-MRI segmentation and adds evidence to the feasibility of subfield-level biomarkers for AD and other neurodegenerative diseases.

Acknowledgements: This work is supported in part by NIH grants K25 AG027785, K23 AG028018, R01 AG010897, R01 AG010897, P01 AG12435, and grant 10295 from the Penn-Pfizer Alliance.

References: [1] Mueller et al., *HBM* 31(9):1339-47 (2010); [2] Wang et al., *Arch General Psych* 67(3):296-303 (2010); [3] Mueller et al., *Epilepsia* 50(6):1474-83 (2009); [4] Yushkevich et al., *Neuroimage* 53(4):1208-24 (2010); [5] Smith et al., *Neuroimage* 23(S1):S208-19; [6] Avants et al, *Med. Image Anal* 12: 26–41 (2008).

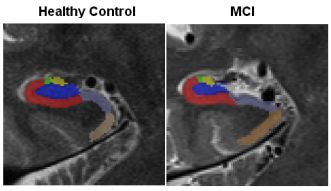

Figure 1. Examples of automatic HF-MRI segmentation

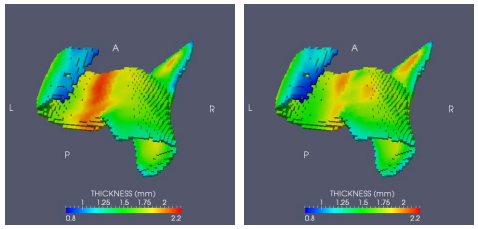

Figure 2. Average thickness maps for controls (left) and MCI patients (right) plotted on the region formed by the subfields PHG, ERC, SUB, CA1, CA2, CA3.

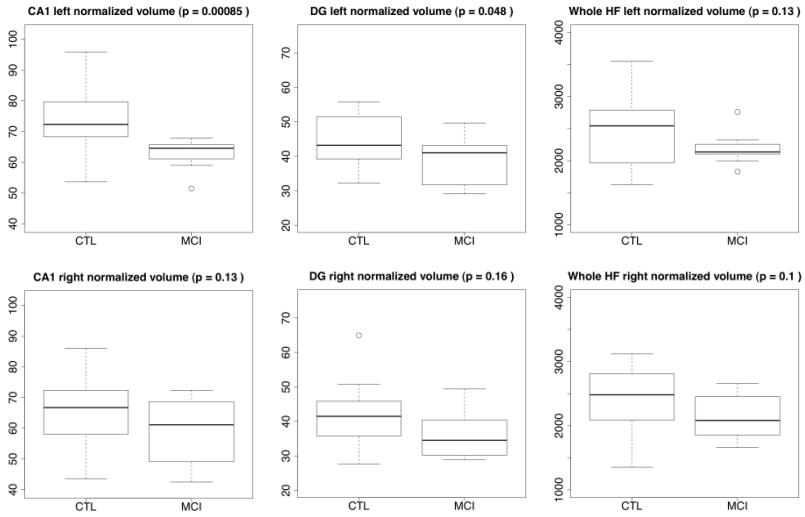

Figure 1. Volume differences between MCI patients and controls in CA1, DG and whole HF.